Prediction of Combustion Driven Pressure Oscillations in a Turbofan Engine Afterburner

Niklas Andersson

Thesis for the degree of Master of Science in Mechanical Engineering
at Chalmers University of Technology

Trollhättan, December 2000

Prediction of Combustion Driven Pressure Oscillations in a Turbo Fan Engine Afterburner

Niklas Andersson

Abstract

The aim of this work was to obtain possible acoustic eigenmodes in a flow field using approximate eigenvalue analysis and find out if those eigenmodes might be augmented by combustion instabilities in the flow field using Rayleigh's criteria. The method that was used is founded on a combination of an approximate eigenvalue analysis method and the linearized Euler equations. The method uses the linearized Euler equations to project the characteristics of the flow field on a Krylov sub space out of which the acoustic eigenmodes are extracted. The method was applied on the afterburner duct of the RM12 gas turbine, the propelling unit of the Gripen fighter, developed and manufactured at Volvo Aero Corporation in Trollhättan, Sweden.

The calculations were performed on a structured mesh and the flow field used for linearization of the Euler equations was interpolated to this mesh from a flow field estimated in the commercial solver Fluent on an unstructured mesh.

The expected result was to find a set of weakly damped eigenmodes but the eigenmodes extracted were all of strongly growing character. This might be caused by the fact that the interpolation routine used makes a quite rough interpolation of the flow field. The interpolated flow field constitutes a not too well converged solution with the solver and mesh used. The eigenmodes estimated corresponds to the course of events taking place after starting the Euler solver with the non-convergent flow field used as start solution, i.e. oscillating residuals and excitation of numerical eigenmodes. Though the eigenmodes were not those expected the frequency with which they oscillate is quite similar to frequencies obtained in earlier calculations made at Volvo with a two-dimensional axisymmetric approach. In this case the mean flow field was estimated using the same mesh as for the linear Euler solver and with a viscous solver of high compatibility.

The importance of using a well-converged mean flow field was investigated by replacing the interpolated flow field with a stagnated flow field. The eigenmodes extracted with this flow field used for linearization of the Euler equations gave more realistic results.

The conclusion of this work is that the mean flow field used is of great importance and that if this method is to be used for engineering purposes a grid-to-grid interpolation routine that ensures convergent solutions on the destination grid has to be developed.

Keywords: Eigenvalue analysis, Arnoldi, Linear Euler, Flow field interpolation, Structured mesh, Rayleigh's criteria, Afterburner, Pressure oscillations, combustion, heat release.

Contents

Acknowledgements

This thesis is the result of a diploma work for the degree of Master of Science at Chalmers University of Technology conducted at the Department of Thermo and Fluid Dynamics. The work was carried out at the Department of Aero-Thermo Dynamics at Volvo Aero Corporation in Trollhättan, Sweden. My supervisor at Volvo was associate professor Lars-Erik Eriksson.

I would like to thank Lars-Erik for taking time to answer my questions and share his great knowledge in fluid dynamics with me. I would also like to express my gratitude to the rest of the employee at the Department of Aero-Thermo Dynamics for their help and kind treatment during the last twenty weeks.

Nomenclature

t	Time	[s]
x_i	Cartesian coordinates	[m]
ρ	Density	[kg/m^3]
u_i	Velocity	[m/s]
p	Pressure	[N/m^2]
T	Temperature	[K]
c	Speed of sound	[m/s]
$Y^{(\alpha)}$	Mass fraction of species α	Dimensionless
k	Turbulent kinetic energy	[J/kg]
ε	Dissipation of turbulent kinetic energy	[J/kg·s]
e_0	Total energy	[J/kg]
e	Internal energy	[J/kg]
h_0	Total enthalpy	[J/kg]
h	Internal enthalpy	[J/kg]
τ_{ij}	Stress tensor	[N/m^2]
q_i	Energy diffusion vector	[J/m^2·s]
$j_i^{(\alpha)}$	Mass diffusion vector, species α	[kg/m^2·s]
$s^{(\alpha)}$	Net production rate, species α	[kg/m^3·s]
R	Mixture gas constant	[J/kg·K]
$R^{(\alpha)}$	Gas constant for species α	[J/kg·K]
R_{univ}	Universal gas constant	[J/kmol·K]
$M^{(\alpha)}$	Molecular weight of species α	[kg/kmol]
$e^{(\alpha)}$	Internal energy, species α	[J/kg]
$h^{(\alpha)}$	Enthalpy, species α	[J/kg]
$\mathrm{H}_\mathrm{f}^{(\alpha)}$	Coeff. In linear approx. of $e^{(\alpha)}$ and $h^{(\alpha)}$	[J/kg]
$C_v^{(\alpha)}$	Coeff. In linear approx. of $e^{(\alpha)}$	[J/kg K]
$C_p^{(\alpha)}$	Coeff. In linear approx. of $h^{(\alpha)}$	[J/kg K]
μ	Laminar viscosity	[Ns/m^2]
μ_t	Turbulent eddy viscosity	[Ns/m^2]
Pr	Laminar Prandtl number	Dimensionless
Pr_t	Turbulent Prandtl number	Dimensionless
Sc	Laminar Schmidt number	Dimensionless
Sc_t	Turbulent Schmidt number	Dimensionless

$C_{\mu} = 0.09$	Constant in k-ε turbulence model	Dimensionless
$C_{\varepsilon 1} = 1.44$	Constant in k-ε turbulence model	Dimensionless
$C_{\varepsilon 2} = 1.92$	Constant in k-ε turbulence model	Dimensionless
$\sigma_{k} = 1.0$	Constant in k-ε turbulence model	Dimensionless
$\sigma_{\varepsilon} = 1.3$	Constant in k-ε turbulence model	Dimensionless

Introduction

Gas turbines used for propulsion of military aircrafts often have an afterburner between the last turbine stage and the propelling nozzle to enhance the thrust for shorter amounts of time. Such an afterburner duct mainly contains fuel injectors and flame holders. The fuel injectors are used to produce fuel droplets, which vaporize fast and mix with the air. The flame holders create recirculation zones in which combustion can be initiated and maintained. At maximum thrust almost all oxygen in the afterburner is consumed by the combustion, i. e. the combustion is almost stoichiometric. This means that large amounts of energy are transformed in the afterburner. Such a large transformation from chemical energy to thermal energy increases the possibility for pressure oscillations. These pressure oscillations occur when a certain acoustic natural oscillation in the afterburner give rise to variations in the combustion rate that is in phase with the pressure variations. Sources of such oscillatory behavior may be, for example, periodic fluctuations in the vaporization of fuel droplets or pressure waves that perturb the flame, causing it to move and change in surface area, thereby altering an instantaneous rate of heat release, Macqiusten et al [17], [18] and Eriksson [9].

According to Rayleigh's criteria acoustic waves gain energy from unsteady heating if the fluctuations in the heat release rate are in phase with the pressure, Eriksson [9]. Transport of energy into the natural oscillation makes the amplitude increase exponentially. Due to non-linear effects the amplitude is restrained to a certain level. This equilibrium amplitude is often harmful for the afterburner considering structural damage.

The lower range of frequencies, typically 50-200 Hz, are characterized as acoustic waves traveling axially along the afterburner and bounded by the turbine and the propelling nozzle, Hendersson et al [13]. These instabilities are known as rumble or reheat buzz. Rumble occurs mainly at high fuel-air ratios and at flight Mach numbers and altitudes where low duct inlet air temperatures and pressure exists, Russel et al [24]. This instability may lead to afterburner blowout, fan surge, engine stall and mechanical failure, Russel et al [24]. Consequently it is of big interest to develop a method for prediction of rumble in the afterburner to be able to avoid this phenomenon when designing or modifying afterburners.

The aim of this thesis is to find eigenmodes with low frequency in the afterburner of the RM12 engine. If such eigenmodes are found stability analysis based on Rayleigh's criteria should be applied on those eigenmodes. A method that has proved to be successful for this kind of problem, Eriksson [9], is a method founded on the linearized Euler equations and an approximate eigenvalue analysis method. The basic idea of the method is that an instantaneous flow field may be expressed as a mean flow field and an instantaneous perturbation field. The mean flow field of the afterburner duct may be estimated with a standard RANS based finite volume code, i.e. a three dimensional Navier-Stokes solver that includes a standard k-ε turbulence model and a reaction model with heat release. For perturbations small enough the Navier-Stokes equations may be linearized about this mean flow field. Assuming that for most of the acoustic related perturbations the diffusive effects may be neglected the augmentation or damping of the acoustic eigenmodes may be governed by the linearized Euler equations.

Calculations of the kind described above have been performed at VAC for an axisymmetric afterburner duct with two-dimensional solvers, Eriksson [9]. In this thesis fully three dimensional calculations are to be performed.

1 Governing equations

In this chapter the equations governing the fluid dynamics of the flows considered in this thesis are presented in tensor form. For further details see Eriksson [7], Hoffman [14], Panton [21] and Versteg [26].

1.1 Viscous flow

The mean flow field in the afterburner duct is considered to be a compressible viscous turbulent reacting flow of ideal gases, which is governed by the Reynolds-averaged Navier-Stokes (RANS) equations. The equations constitute a set of transport equations governing transport of mass, momentum and energy.

$$\frac{\partial \rho}{\partial t} + \frac{\partial}{\partial x_j}\left[\rho u_j\right] = 0 \tag{1.1}$$

$$\frac{\partial}{\partial t}\left(\rho u_i\right) + \frac{\partial}{\partial x_j}\left[\rho u_i u_j + P\delta_{ij} - \tau_{ij}\right] = 0 \tag{1.2}$$

$$\frac{\partial}{\partial t}\left(\rho e_0\right) + \frac{\partial}{\partial x_j}\left[\rho u_j h_0 + q_j - u_i \tau_{ij}\right] = 0 \tag{1.3}$$

In (1.2) and (1.3) τ_{ij} is the viscous stress obtained by using the Boussinesque assumption and is defined by

$$\tau_{ij} = \left(\mu + \mu_t\right)\left[\frac{\partial u_i}{\partial x_j} + \frac{\partial u_j}{\partial x_i} - \frac{2}{3}\frac{\partial u_k}{\partial x_k}\delta_{ij}\right] - \frac{2}{3}\rho k \delta_{ij} \tag{1.4}$$

The eddy viscosity is defined by

$$\mu_t = C_\mu \rho \frac{k^2}{\varepsilon} \tag{1.5}$$

Assuming Fourier's heat law to be valid, the heat flux including heat release may be expressed as

$$q_j = -\lambda \frac{\partial T}{\partial x_j} + \sum_{\alpha=1}^{m} h^{(\alpha)} j_j^{(\alpha)} = -C_p\left(\frac{\mu}{Pr} + \frac{\mu_t}{Pr_t}\right)\frac{\partial T}{\partial x_j} + \sum_{\alpha=1}^{m} h^{(\alpha)} j_j^{(\alpha)} \tag{1.6}$$

where the mass diffusion vector for species α is defined by

$$j_j^{(\alpha)} = -\left(\frac{\mu}{Sc} + \frac{\mu_t}{Sc_t}\right)\frac{\partial}{\partial x_j} Y^{(\alpha)} \tag{1.7}$$

The change in mass fraction of species α due to convection, diffusion and chemical reaction is governed by the conservation equation below.

$$\frac{\partial Y^{(\alpha)}}{\partial t} + \frac{\partial}{\partial x_j}\left[\rho u_j Y^{(\alpha)} + j_j^{(\alpha)}\right] = s^{(\alpha)} \tag{1.8}$$

To be able to model turbulent effects in the flow a turbulence model has to be used. A turbulence model often used is the standard k-ε model. To implement the turbulence model transport equations for the turbulence quantities are needed. Turbulent kinetic energy and dissipation of turbulent kinetic energy are the two turbulent quantities modeled.

$$\frac{\partial k}{\partial t} + \frac{\partial}{\partial x_j}\left[\rho u_j k - \left(\mu + \frac{\mu_t}{\sigma_k}\right)\frac{\partial k}{\partial x_j}\right] = P_k - \rho\varepsilon \tag{1.9}$$

$$\frac{\partial \varepsilon}{\partial t} + \frac{\partial}{\partial x_j}\left[\rho u_j \varepsilon - \left(\mu + \frac{\mu_t}{\sigma_\varepsilon}\right)\frac{\partial \varepsilon}{\partial x_j}\right] = \left(C_{\varepsilon_1} P_k - C_{\varepsilon_1}\rho\varepsilon\right)\frac{\varepsilon}{k} \tag{1.10}$$

For the standard k-ε turbulence model the following expression for the production of turbulent kinetic energy is used.

$$P_k = \left[\mu_t\left(\frac{\partial u_i}{\partial x_j} + \frac{\partial u_j}{\partial x_i} - \frac{2}{3}\frac{\partial u_k}{\partial x_k}\delta_{ij}\right) - \frac{2}{3}\rho k \delta_{ij}\right]\frac{\partial u_i}{\partial x_j} \tag{1.11}$$

In order to close this system of partial differential equations assumptions are made concerning the thermodynamics of the gases. It is assumed that the gas mixture behaves as a perfect gas, i.e. that it obeys the gas law.

$$P = \rho R T \tag{1.12}$$

Where the total gas constant of the gas mixture is the sum of the gas constant for each species multiplied with corresponding mass fraction.

$$R = \sum_{\alpha=1}^{m} Y^{(\alpha)} R^{(\alpha)} \tag{1.13}$$

The gas constant for each species is defined by

$$R^{(\alpha)} = \frac{R_{univ}}{M^{(\alpha)}} \tag{1.14}$$

Where R_{univ} is the universal gas constant and $M^{(\alpha)}$ is the molar mass of species α.

It is also assumed that the gas is in vibrational equilibrium, i.e. that the internal energy and enthalpy are functions of the gas composition and temperature according to

$$e = \sum_{\alpha=1}^{m} Y^{(\alpha)} e^{(\alpha)}(T) \tag{1.15}$$

and

$$h = \sum_{\alpha=1}^{m} Y^{(\alpha)} h^{(\alpha)}(T) \tag{1.16}$$

The internal energy and enthalpy for each species α are functions of the temperature only. The individual internal energies and enthalpies are assumed to be absolute quantities, i.e. they are assumed to contain the heat of formation. In real flows the temperature dependence of the internal energy and enthalpy is often non-linear, but in many cases it is possible to work with linearized relations adjusted to suit a certain temperature range. The linearized relations for internal energy and enthalpy respectively are given in (1.17) and (1.18).

$$e^{(\alpha)} = H_f^{(\alpha)} + C_v^{(\alpha)} \cdot T \tag{1.17}$$

$$h^{(\alpha)} = H_f^{(\alpha)} + C_p^{(\alpha)} \cdot T \tag{1.18}$$

The relation between specific heat for constant pressure and volume respectively for species α are given by (1.19).

$$C_p^{(\alpha)} = C_v^{(\alpha)} + R^{(\alpha)} \tag{1.19}$$

From the thermodynamic relations above the auxiliary relations, (1.20)-(1.22), are obtained.

$$e = H_f + C_v \cdot T \tag{1.20}$$

$$h = H_f + C_p \cdot T \tag{1.21}$$

$$h = e + \frac{p}{\rho} \tag{1.22}$$

The total heat of formation and the specific heats for the entire gas mixture are obtained analogous to the internal energy and enthalpy.

$$H_f = \sum_{\alpha=1}^{m} Y^{(\alpha)} H_f^{(\alpha)} \tag{1.23}$$

$$C_v = \sum_{\alpha=1}^{m} Y^{(\alpha)} C_v^{(\alpha)} \tag{1.24}$$

$$C_p = \sum_{\alpha=1}^{m} Y^{(\alpha)} C_p^{(\alpha)} \tag{1.25}$$

The relation between the specific heats is for the entire gas mixture as for each single species defined by

$$C_p = C_v + R \tag{1.26}$$

It should be noted that the equations governing the conservation of species, (1.8), only include *m-1* transport equations, where *m* is the total number of species. The reason is that the consistency relations, (1-27) – (1.29), make the last equation redundant. The sum of all *m* species transport equations reduces to the usual continuity equation, (1.1).

$$\sum_{\alpha=1}^{m} Y^{(\alpha)} = 1 \tag{1.27}$$

$$\sum_{\alpha=1}^{m} j_i^{(\alpha)} = 0 \tag{1.28}$$

$$\sum_{\alpha=1}^{m} s^{(\alpha)} = 0 \tag{1.29}$$

1.2 The Euler equations for inviscid flow

For high Reynolds number flows, Re≈10^4 and higher, most viscous effects takes place in thin boundary layers, shear layers and wakes. That is a large part of the flow will have an inviscid character. The Euler equations are obtained from the Navier-Stokes equations by assuming zero viscosity, i.e. disregard the diffusive parts of the governing equations. The Euler equations describe the hyperbolic nature of the flow, i.e. the convection of various types of waves such as entropy waves, vorticity waves and acoustic waves. A small amount of viscosity only adds a slight diffusion of these phenomena [8]. Thus the Euler equations, governing compressible flow with multi species, may be expressed as below.

$$\frac{\partial \rho}{\partial t} + \frac{\partial}{\partial x_j}\left[\rho u_j\right] = 0 \tag{1.28}$$

$$\frac{\partial}{\partial t}\left(\rho u_i\right) + \frac{\partial}{\partial x_j}\left[\rho u_i u_j + P\delta_{ij}\right] = 0 \tag{1.29}$$

$$\frac{\partial}{\partial t}\left(\rho e_0\right) + \frac{\partial}{\partial x_j}\left[\rho u_j h_0\right] = 0 \tag{1.30}$$

$$\frac{\partial Y^{(\alpha)}}{\partial t} + \frac{\partial}{\partial x_j}\left[\rho u_j Y^{(\alpha)}\right] = 0 \tag{1.31}$$

Further on in the report the Euler equations on conservative form will be written in a more manageable compact form.

$$\frac{\partial Q}{\partial t} + \frac{\partial F_j}{\partial x_j} = 0 \tag{1.32}$$

where

$$Q = \begin{bmatrix} \rho \\ \rho u_i \\ \rho e_0 \\ \rho Y^{(\alpha)} \end{bmatrix}, \quad F_j = \begin{bmatrix} \rho u_j \\ \rho u_i u_j + P\delta_{ij} \\ \rho u_j h_0 \\ \rho u_j Y^{(\alpha)} \end{bmatrix} \tag{1.33}$$

2 Linearization of the Euler equations

In the final part of the previous chapter the non-linear Euler equations were introduced.

$$\frac{\partial Q}{\partial t}+\frac{\partial F_j}{\partial x_j}=0 \tag{2.1}$$

The first step in linearization of the Euler equations is to assume that the instantaneous flow field may be expressed as the sum of a time averaged flow field and an instantaneous perturbation field.

$$Q=Q_0+Q' \tag{2.2}$$

where Q' is the perturbation vector containing perturbations of all properties.

$$Q'=\begin{bmatrix}\rho' \\ (\rho u_i)' \\ (\rho e_0)' \\ \left(\rho Y^{(\alpha)}\right)'\end{bmatrix} \tag{2.3}$$

Inserting (2.2) in (2.1) gives

$$\frac{\partial Q_0}{\partial t}+\frac{\partial Q'}{\partial t}+\frac{\partial}{\partial x_j}F_j\left[Q_0+Q'\right]=0 \tag{2.4}$$

The fluxes F_j are estimated with Taylor series.

$$F_j\left[Q_0+Q'\right]=F_j\left(Q_0\right)+\left(\frac{\partial F_j}{\partial Q}\right)_0 Q'+........ \tag{2.5}$$

In (2.5) $\left(\frac{\partial F_j}{\partial Q}\right)_0$ is a derivative calculated in the time averaged flow field. Inserting (2.5) in (2.4) gives

$$\frac{\partial Q_0}{\partial t}+\frac{\partial Q'}{\partial t}+\frac{\partial F_{0j}}{\partial x_j}+\frac{\partial}{\partial x_j}\left[\left(\frac{\partial F_j}{\partial Q}\right)_0 Q'\right]=0 \tag{2.6}$$

Since the averaged part of (2.5) by definition is zero the equations reduces to

$$\frac{\partial Q'}{\partial t} + \frac{\partial}{\partial x_j}\left[\left(\frac{\partial F_j}{\partial Q}\right)_0 Q'\right] = 0 \qquad (2.7)$$

Which are the linearized Euler equations on conservative form. To make the expressions more manageable a new flux term is introduced.

$$F_{LE\,j} = \left[\left(\frac{\partial F_j}{\partial Q}\right)_0 Q'\right] \qquad (2.8)$$

Inserting (2.8) in (2.7) gives

$$\frac{\partial Q'}{\partial t} + \frac{\partial F_{LE\,j}}{\partial x_j} = 0 \qquad (2.9)$$

When proceeding with the development of the code there are two alternatives. The first is to apply finite volume directly on (2.7) and the second is to linearize a finite volume code for non-linear equations. Since non of the alternatives are more accurate then the other and a finite volume code for the non-linear Euler equations already exists at VAC the later alternative is chosen. By doing it this way one gets high compatibility between the non-linear and the linear solver.

3 Boundary conditions

To ensure good calculation results it is of great importance to use well-posed boundary conditions. Below a method of finding such boundary conditions is described. For further details see Eriksson [7] and [8].

3.1 Boundary conditions based on characteristic variables

Information flow across inflow and outflow boundaries is determined by the behavior of local planar waves traveling in a direction normal to the surface. This information flow is entirely described by the sign of the characteristic speed corresponding to each characteristic variable. The boundary conditions based on the characteristic variables are obtained by one-dimensional analysis of the Euler equations at the boundary.

The first step is to derive the Euler equations based on characteristic variables. For smooth solutions the Euler equations may be written in an alternative quasi-linear form.

$$\frac{\partial Q}{\partial t} + A\frac{\partial Q}{\partial x} + B\frac{\partial Q}{\partial y} + C\frac{\partial Q}{\partial z} = 0 \tag{3.1}$$

Where

$$A = \frac{\partial F_x}{\partial x}\ ,\ B = \frac{\partial F_y}{\partial y}\ ,\ C = \frac{\partial F_z}{\partial z} \tag{3.2}$$

A, B and C are the flux Jacobian matrices of each convective term. For small perturbations in a local region the flux Jacobain matrixes may be frozen and a linear equation is obtained. Assuming that the perturbations corresponds to planar waves in space, all with the wave planes normal to the unit vector (α,β,γ) for which $\alpha^2 + \beta^2 + \gamma^2 = 1$, a simplified linear relation is obtained

$$\frac{\partial Q}{\partial t} + \tilde{A}\frac{\partial Q}{\partial \xi} = 0 \tag{3.3}$$

where $\tilde{A}$ is a linear combination of the different Jacobian flux terms and ξ is the space variable in the direction normal to the wave plane.

$$\tilde{A} = \alpha A + \beta B + \gamma C \tag{3.4}$$

and

$$\xi = \alpha x + \beta y + \gamma z \tag{3.5}$$

This system of coupled equations describes the propagation of the waves along the ξ-axis. The system may be decoupled using a set of characteristic variables.

$$Q = TW \ , W = \begin{bmatrix} w^{(1)} \\ w^{(2)} \\ w^{(3)} \\ w^{(4)} \\ w^{(5)} \end{bmatrix} \tag{3.6}$$

where $w^{(1)}, \ldots, w^{(5)}$ are characteristic variables. T and T^{-1} are matrices that diagonalize $\tilde{A}$ according to

$$T^{-1}\tilde{A}T = \Lambda = \begin{bmatrix} \lambda^{(1)} & 0 & 0 & 0 & 0 \\ 0 & \lambda^{(2)} & 0 & 0 & 0 \\ 0 & 0 & \lambda^{(3)} & 0 & 0 \\ 0 & 0 & 0 & \lambda^{(4)} & 0 \\ 0 & 0 & 0 & 0 & \lambda^{(5)} \end{bmatrix} \tag{3.7}$$

The physical interpretation of the characteristic variables is

$w^{(1)}$	= entropy wave
$w^{(2)}, w^{(3)}$	= vorticity waves
$w^{(4)}, w^{(5)}$	= acoustic waves

Each characteristic variable $w^{(\alpha)}$ is traveling along the ξ-axis with the corresponding characteristic speed $\lambda^{(\alpha)}$. The five eigenvalues or characteristic speeds may be found to be

$$\begin{aligned} &\lambda^{(1)} = \lambda^{(2)} = \lambda^{(3)} = \alpha u + \beta v + \gamma w \\ &\lambda^{(4)} = \alpha u + \beta v + \gamma w + c\sqrt{\alpha^2 + \beta^2 + \gamma^2} \\ &\lambda^{(5)} = \alpha u + \beta v + \gamma w - c\sqrt{\alpha^2 + \beta^2 + \gamma^2} \end{aligned} \tag{3.8}$$

Using the relations above the expression (3.3) may be transformed to

$$\frac{\partial W}{\partial t} + \Lambda \frac{\partial W}{\partial \xi} = 0 \tag{3.9}$$

which is an uncoupled system of five transport equations. All planar waves normal to a given direction may be represented by the scalar transport of five characteristic variables, each with its own speed. The five characteristic speeds describe the flow of information and are thus of importance in formulation of inflow and outflow boundary conditions. If a characteristic speed is less than zero at the boundary the corresponding planar wave is traveling into the domain. Information about the in going characteristic variables has to be specified from the exterior. If a characteristic speed is larger or equal to zero the corresponding planar wave is traveling towards the boundary out of the domain. In this case no information about the characteristic variable has to be specified. Strict adherence to these principles results in zero-order non-reflecting boundary conditions.

A less strict principle is to specify other variables than the characteristic variables at a boundary, but taking care that the number of specified variables is the same as the number of ingoing characteristic variables. This treatment of the boundaries does not give absorbing or non-reflecting boundary conditions and does not guarantee a well-posed boundary condition. Certain combinations of variables are known to be safe.

4 Approximate eigenvalue analysis

Eigenvalue analysis is to be used when studying the acoustic behavior of the afterburner duct. The number of eigenvalues needed for a complete description of the behavior of a system is of course equal to the number of degrees of freedom of the same system. Most often it is extremely expensive, if not impossible, to obtain all the eigenvalues due to numerous degrees of freedom. The aim of this work is to find acoustic eigenmodes in a given flow field which, if augmented, may lead to structural damage. The eigenmodes of interest are those that grow in time and those that are among the least damped of the damped eigenmodes. Thus one needs a method that extracts eigenmodes with certain characteristics out of a large linear system. According to Eriksson [9] this may be done with an eigenvalue extraction routine called Arnoldi's method combined with a linear Euler solver.

4.1 Arnoldi's method

The idea of Arnoldi's method is to extract the eigenvalues for a set of equations obtained from the large linear system that is to be analyzed. This gives a set of approximate eigenvalues for the actual system. The method has the advantage that one does not need to have access to the matrix, which is to be examined, explicitly, Eriksson [9]. It is sufficient if the matrix may be defined implicitly as

$$Y = A \cdot X \tag{4.1}$$

That is for an arbitrary vector *X* it is possible to obtain the vector *Y* with the matrix *A* working as an operator on *X*. A set of vectors, such as *Y*, that has been obtained using the linear operator *A* builds a Krylov subspace that is used in Arnoldi's method when extracting approximate eigenvalues of the matrix *A*, i.e. an approximate solution to the eigenvalue problem

$$Az = \lambda z \tag{4.2}$$

The matrix *A* is an *n*x*n* matrix and *z* is a vector with *n* elements. The characteristics of the matrix *A* are projected on a Krylov subspace, K_m, using the sequence described in (4.3), Eriksson [10].

$$\begin{aligned}&\text{Start vector } P_1\\ &P_{k+1} = AP_k \;;\; k = 1, 2, \ldots, m-1 \;;\; m << n\end{aligned} \tag{4.3}$$

The vectors P_1 to P_m constitute the Krylov subspace, which is an *n*x*m* matrix.

$$K_m = \begin{bmatrix} \begin{bmatrix} \\ P_1 \\ \\ \end{bmatrix} & \begin{bmatrix} \\ P_2 \\ \\ \end{bmatrix} & \cdots & \begin{bmatrix} \\ P_m \\ \\ \end{bmatrix} \end{bmatrix} \tag{4.4}$$

An upper Hessenberg matrix, H_m, is obtained by combine the Krylov sequence with orthogonalization. This may be expressed with the following algorithm, Eriksson [10].

Start vector P_1

$e_1 = P_1 / \|P_1\|$

for k=1 to m

$$P_{k+1} = Ae_k - \sum_{j=1}^{k} h_{j,k} e_j \text{ , where } h_{j,k} = Ae_k \cdot e_j \tag{4.5}$$

$$h_{k+1,k} = \|P_{k+1}\|$$

$$e_{k+1} = P_{k+1} / h_{k+1,k}$$

end

The coefficients $h_{j,k}$ define the upper Hessenberg matrix H_m.

$$\begin{bmatrix} h_{11} & h_{12} & h_{13} & & \cdots & h_{1m} \\ h_{21} & h_{22} & h_{23} & & \cdots & h_{2m} \\ 0 & h_{32} & h_{33} & & \cdots & h_{3m} \\ 0 & 0 & h_{43} & & \cdots & h_{4m} \\ \vdots & \vdots & & \ddots & & \vdots \\ 0 & 0 & \cdots & 0 & h_{mm-1} & h_{mm} \end{bmatrix}, \ m \times m, \ m << n \tag{4.6}$$

The eigenvalues of H_m are the desired approximate eigenvalues of A and the eigenvectors of H_m define the corresponding eigenvectors of A.

$$H_m v_j = \tilde{\lambda} v_j$$
$$\tilde{u}_j = \sum_{k=1}^{m} (v_j)_k \ e_k \tag{4.7}$$

Since the upper Hessenberg matrix is real the eigenvalues will be represented as complex conjugated couples.

In this thesis the acoustic behavior of a flow field is to be studied. If there are no perturbations on the inflow or outflow of the calculation domain the problem is homogenous. That is if an initial perturbation field is added to the mean flow field the development of those perturbations in time is linear. The time differentiation may be expressed as

$$\frac{d}{dt}\begin{bmatrix} Q'_{Cell_1} \\ Q'_{Cell_2} \\ \vdots \\ Q'_{Cell_{Ncells}} \end{bmatrix} = M \begin{bmatrix} Q'_{Cell_1} \\ Q'_{Cell_2} \\ \vdots \\ Q'_{Cell_{Ncells}} \end{bmatrix} \tag{4.8}$$

In (4.2) Q'_{Cell_n} is a vector containing perturbations of all variables in cell number *n* and the matrix *M* is a large square matrix describing the linear development of the perturbations in time. The solution to this linear system is completely described by the eigenvectors and eigenvalues belonging to *M*.

For convenience the following notation is introduced

$$Q' = \begin{bmatrix} Q'_{Cell_1} \\ Q'_{Cell_2} \\ \vdots \\ Q'_{Cell_{Ncells}} \end{bmatrix} \tag{4.9}$$

Introducing *Q'* (4.2) may be rewritten as

$$\frac{d}{dt} Q' = M\ Q' \quad \text{or} \quad Q'(t_0 + \tau) = \left[e^{M\tau}\right] Q'(t_0) \tag{4.10}$$

Which actually is an expression of the same form as (4.1) and Arnoldi's method is applicable on the problem of finding eigenmodes of the linear operator $\left[e^{M\tau}\right]$.

Arnoldi's method is applied on the matrix or linear operator $\left[e^{M\tau}\right]$ but it is actually the eigenvalues and eigenvectors of the matrix *M* that is of interest. If λ is an eigenvalue of the matrix *M*, $e^{\lambda\tau}$ is the corresponding eigenvalue to the matrix $\left[e^{M\tau}\right]$. Thus the eigenvalues of the matrix *M* is obtained as

$$\hat{\lambda} = e^{\lambda\tau} \Rightarrow \lambda = \frac{1}{\tau} ln\hat{\lambda} \tag{4.11}$$

Eigenvalues and eigenvectors of the matrix M give information about the acoustic eigenmodes of the system. Assume that any perturbation eigenmode may be expressed as

$$Q' = A e^{\lambda t} z \tag{4.12}$$

Where A is the amplitude and λ and z are the eigenvalue and eigenvector belonging to the eigenmode. Time differentiation of (4.12) shows that it is a valid solution.

$$\frac{\partial}{\partial t} Q' = \lambda \mathrm{A}\, \mathrm{e}^{\lambda t} z = \{M z = \lambda z\} = M \mathrm{A}\, \mathrm{e}^{\lambda t} z = M Q' \tag{4.13}$$

The perturbation field may be expressed as a linear combination of eigenmodes

$$Q' = \sum_k A_k e^{\lambda_k t} z_k \tag{4.14}$$

As mentioned before the eigenvalues comes out as complex conjugated couples. The argument of a complex eigenvalue defines the frequency with which the corresponding eigenmode is oscillating. The mapping of the eigenvalues of the matrix $\left[e^{M\tau}\right]$ to the eigenvalues of the matrix M makes it quite difficult to know with which frequency the corresponding eigenmode is oscillating, see figure 1. First of all it may be any of the two frequencies corresponding directly to the arguments of the complex conjugated couple. If none of those frequencies is right it may be any frequencies corresponding to any multiple of 2π plus the arguments.

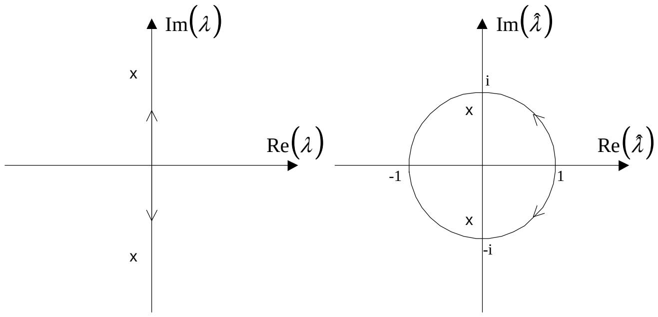

Figure 1 *Spectrum of M and* $e^{M\tau}$

4.2 Arnoldi's method combined with linear Euler

It has been shown that the accuracy of the approximate spectrum obtained is best for the outer parts of the spectrum of the matrix studied whereas the inner parts are poorly represented [10]. The inner parts of the spectrum get more accurate as the dimension of the Krylov subspace approaches the dimension of the matrix studied. Since the whole idea of using Arnoldi's method is to be able to find interesting approximate eigenvalues for a matrix with much smaller dimensions than the actual matrix studied the method has to be used together with a spectrum transformation algorithm that is capable of moving the interesting parts of the spectrum outwards. To be able to transform the spectrum of the matrix *M* in the way described above one need a process which march the linearized discretized system in time with $Q'(t_0)$ as start solution and $Q'(t_0+\tau)$ as final solution, which represents the function of the matrix $\left[e^{M\tau}\right]$. At the same time the process has to result in a movement of the interesting parts outwards in the spectrum. The process used for this purpose is a linear Euler solver, which acts as an operator that each times used marches the input vector *k* time steps each Δt long forward in time with a three-stage Runge-Kutta method, se figure 2. The linear Euler operator is further on denoted $P_k(\Delta t)$.

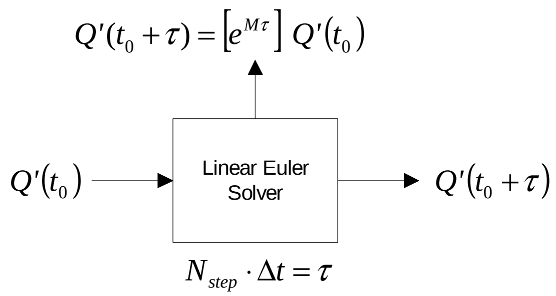

Figure 2 *The linear Euler solver.*

Every complete time step with the Runge-Kutta method is an approximation of an exact integration from time t to $t+\Delta t$, Eriksson [9].

$$Q'_{n+1}=\left[\mathrm{I}+\Delta \mathrm{t} M+\frac{1}{2}(\Delta \mathrm{t})^2 M^2+\frac{1}{4}(\Delta \mathrm{t})^3 M^3\right] Q'_n \tag{4.12}$$

The expression above is the result of three consecutive stages, which are described in more detail in chapter 5.3. The operator $P_k(\Delta t)$ can now be defined according to

$$\mathrm{P_k}(\Delta \mathrm{t})Q'=\left[\mathrm{I}+\Delta \mathrm{t} M+\frac{1}{2}(\Delta \mathrm{t})^2 M^2+\frac{1}{4}(\Delta \mathrm{t})^3 M^3\right]^{\mathrm{k}} Q' \tag{4.13}$$

If a matrix *B* is defined as

$$B=P_k(\Delta t) \tag{4.14}$$

The eigenvalues of B and those of M have the following relation

$$\lambda_B = \left[1 + \Delta t\, \lambda_M + \frac{1}{2}\left(\Delta t\, \lambda_M\right)^2 + \frac{1}{4}\left(\Delta t\, \lambda_M\right)^3 \right]^k \tag{4.15}$$

The relation between the eigenvalues of the both matrixes defines a transformation of the spectrum of the matrix M such that the least damped eigenmodes will be situated furthest from the origin and vice versa for the most damped modes. The selection of time step Δt is determined by the stability limit of the Runge-Kutta method.

5 Numerical method

The solver used is a three-dimensional multi block linear Euler solver for multi species and compressible flow. The convective parts are discretized using a standard cell centered finite volume scheme with third order upwind biasing. A three-stage Runge-Kutta scheme is used for marching in time. For more details concerning the numerical scheme see Eriksson [7].

5.1 Space discretization

The governing equations are discretized on a structured non-orthogonal multi block boundary fitted grid using a cell centered finite volume scheme. The spatial discretization is obtained by integrating the conservation laws (2.9) over a grid cell.

$$\int_{\Omega} \frac{\partial Q'}{\partial t} dV + \int_{\Omega} \frac{\partial FLE_j}{\partial x_j} dV = 0 \tag{5.1}$$

Assuming that the domain Ω is independent of time and using Gauss theorem on the second term (5.1) may be rewritten in the following form

$$\frac{d}{dt} \int_{\Omega} Q' dV + \int_{\partial\Omega} FLE_j \cdot dS_j = 0 \tag{5.2}$$

In words (5.2) says that the rate of change of the cell state vector is equal to the sum of all fluxes across the boundary of the domain Ω.

The flux term can be rewritten as the sum of the fluxes through each face of the cell Ω.

$$\int_{\partial\Omega} FLE_j \cdot dS_j = \sum_{face=1}^{6} \int_{face} FLE_j \cdot dS_j \tag{5.3}$$

Assuming that FLE_j on each face is constant the net flux may be expressed as

$$\sum_{face=1}^{6} \int_{face} FLE_j \cdot dS_j = \sum_{face=1}^{6} FLE_j^{face} \cdot S_j^{face} \tag{5.4}$$

The cell volume averaged state vector is obtained as

$$\overline{Q'}_{\Omega} = \frac{1}{V_{\Omega}} \int_{\Omega} Q' dV \tag{5.5}$$

where V_{Ω} is the cell volume

$$V_{\Omega} = \int_{\Omega} dV \tag{5.6}$$

Inserting the cell averaged state vector (5.5) and the net flux (5.4) into (5.2) gives

$$V_{\Omega} \frac{d}{dt} \overline{Q'}_{\Omega} + \sum_{face=1}^{6} FLE_{j}^{face} \cdot S_{j}^{face} = 0 \tag{5.7}$$

5.2 Convective flux scheme

The convective terms in the conservation equations (5.7) are estimated using a four node characteristic variable based scheme with user controlled upwind biasing. Third order upwind scheme is standard. A more detailed description can be found in [7].

5.3 Time marching

A three dimensional explicit Runge-Kutta scheme is used to proceed in time. The space discretisized (2.7) yields a set of equations, which may be described as

$$V \frac{\Delta Q'}{\Delta t} = -Net\ Flux \tag{5.8}$$

where

$$Net\ Flux = \sum_{face=1}^{6} FLE_{j}^{face} \cdot S_{j}^{face} \tag{5.9}$$

The state vector one step forward in time, Q'_{n+1}, is obtained from the state vector at previous time step, Q'_{n+1}, in three stages.

$$\begin{aligned} Q'_{*} &= Q'_{n} + \Delta t \frac{1}{V} \left(- Net\ Flux\right)\Big|_{Q'_{n}} \\ Q'_{**} &= \frac{1}{2} Q'_{n} + \frac{1}{2} Q'_{*} + \frac{1}{2} \Delta t \frac{1}{V} \left(- Net\ Flux\right)\Big|_{Q'_{*}} \\ Q'_{n+1} &= \frac{1}{2} Q'_{n} + \frac{1}{2} Q'_{*} + \frac{1}{2} \Delta t \frac{1}{V} \left(- Net\ Flux\right)\Big|_{Q'_{**}} \end{aligned} \tag{5.10}$$

6 Verification of the eigenmode extraction routine

To verify the method described above, which uses Arnoldi's method for eigenvalue extraction combined with a linear Euler solver as a spectrum transforming routine to extract the least damped eigenmodes in a domain, the method was applied on a simple test case. The idea is to try to find the least damped eigenmodes in an organ pipe. The organ pipe was approximated with a pipe with one closed and one open end. The length of the pipe was set to one meter and the radius 0.2 meters. The mean flow field which to linearize the Euler equations about was assumed to be stationary air with the following physical properties:

$$
\begin{aligned}
P &= 1 \quad [\text{bar}] \\
T &= 288 \ [\text{K}] \\
C_P/C_V &= 1.4 \\
R &= 287 \ [\text{J/kg K}]
\end{aligned}
$$

The calculation domain consists of a three dimensional one block structured mesh with 51x11x5 nodes, which represent a 10˚ sector of the organ pipe, figure 3. This gives a total of 2000 cells and 10000 degrees of freedom. The time step used in the linear Euler solver where set to the largest time step for which the solver were stable. The solver were found to be stable for the time step $\Delta t = 15\ \mu s$. Each time used in the Arnoldi routine the linear Euler solver made 100 iterations. As a start vector in the Krylov-Hessenberg sequence a perturbation field that were the result of 10000 iterations with the linear Euler solver after an initial perturbation in ρu was used. In the Krylov sequence 90 perturbation fields were obtained and thus the number of degrees of freedom were set to 90. The dimension of the Krylov sub space should be compared to total number of degrees of freedom for the system. The boundary conditions used where solid walls for all boundaries except for the open end where a subsonic outlet boundary condition where used. A subsonic outlet has one ingoing characteristic variable and it has been shown that it makes a well-posed boundary condition to specify the pressure at the outlet, Eriksson [8].

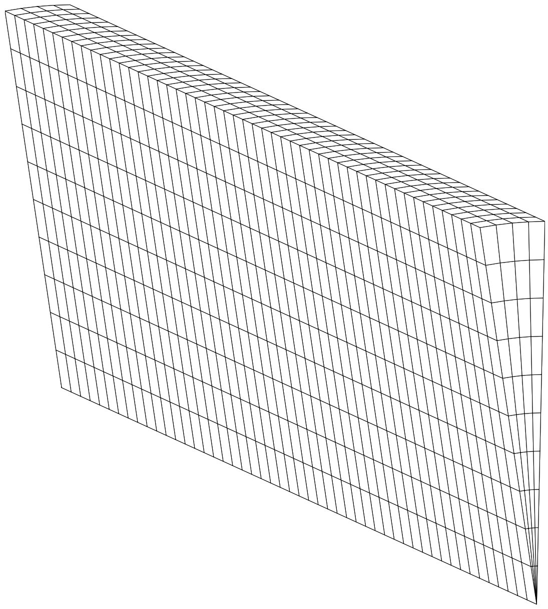

Figure 3 *10˚ sector of the organ pipe.*

Of the total 90 extracted eigenmodes the five of the least damped eigenmodes corresponding to the five first theoretical eigenmodes of an organ pipe were analyzed further and compared with the theoretical modes.

Eigenmode	Theoretical wave length [Pipe lengths]	Theoretical frequency [Hz]	Estimated frequency [Hz]	Eigenmode damping [Amplification/Period]
1	4	85.0	84.6	0.9995
2	4/3	255.0	253.4	0.9992
3	4/5	425.0	422.5	0.9990
4	4/7	595.0	591.2	0.9981
5	4/9	765.0	759.8	0.9978

Table 1 *Frequencies of the extracted eigenmodes compared with the theoretical ones.*

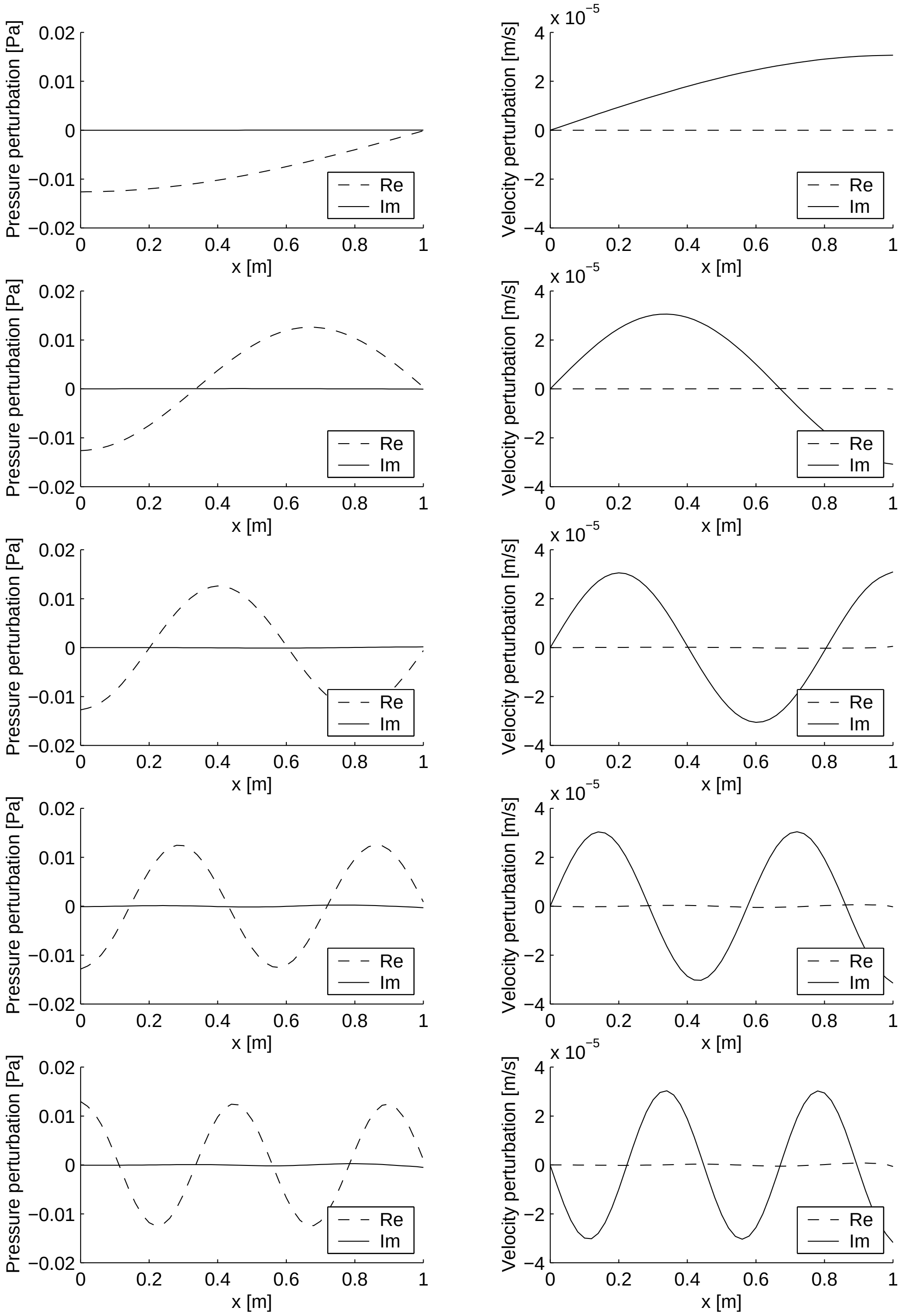

Figure 4 *The figure shows the five least damped eigenmodes of an organ pipe extracted with Arnoldi's method. The pictures to the left and those to the right show real part and imaginary part of the pressure perturbation and velocity perturbation respectively.*

7 Test case

The previous described method for extraction of eigenmodes is applied on the afterburner duct of the RM12 gas turbine, see figure 5.

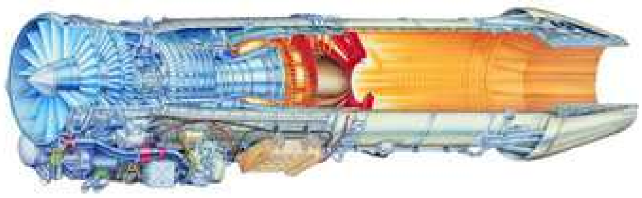

Figure 5 *The RM12 gas turbine.*

The RM12 engine is the propelling unit of the Gripen fighter. The engine is assembled and partially manufactured at Volvo Aero Corporation in Trollhättan and is an enhancement of the F404 engine. The F404 gas turbine is a military power unit developed by General Electric.

The afterburner of a military gas turbine is used for thrust enhancement for shorter periods of time. In figure 6 a schematic outline of the RM12 gas turbine is shown. Air entering the gas turbine is compressed in two compressors, the fan and the high-pressure compressor. The fan consists of three compressor stages and the high-pressure compressor consists of seven. Some of the air compressed in the fan is bled off in the bypass channel. After the high-pressure compressor the air enters the annular combustion chamber where fuel is injected and combusted. The hot exhaust is expanded in two single stage turbines. The high-pressure turbine is driving the high-pressure compressor and the low-pressure turbine is driving the fan. The afterburner duct is situated in the rear part of the engine. Exhaust from the combustion chamber that has expanded through the two turbine stages, enters the afterburner duct and mixes with a smaller amount of colder air bled from the bypass channel. To anchor the combustion flames in the afterburner duct a flame holder system consisting of twelve radial flame holder elements and an axisymmetric inner ring is placed in the afterburner. In the wake regions of this flame holder system combustion may be initiated and maintained. Every second radial flame holder element contains vaporization pipes in which the fuel is vaporized and brought to the wake region of the inner ring. When the afterburner is to be ignited fuel is injected ahead of the flame holders in such way that some of the fuel is distributed around the radial flame holders and burned in the wake regions behind them and some of the fuel is vaporized inside the radial flame holder and burned in the wake region of the inner ring. Due to the fact that the fuel pressure is rather high the amount of fuel injected is approximate constant in time. Pressure fluctuations in the flow field in combination with constant fuel mass flow leads to fluctuations in equivalence ratio. Such fluctuations may lead to unsteady combustion and heat release variations. If the heat release variations is in phase with the pressure variations of the flow field the oscillatory behavior of the field is augmented.

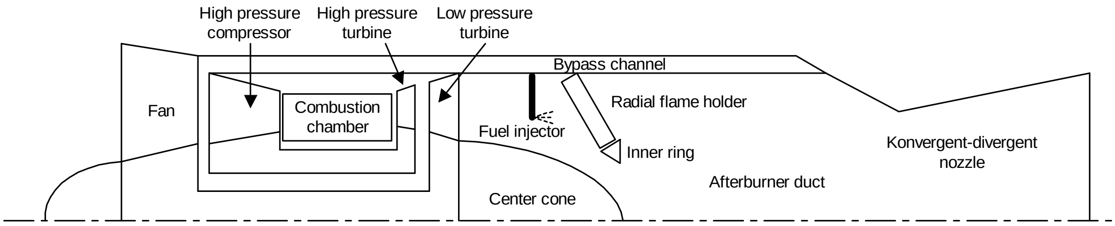

Figure 6 *A schematic outline of the RM12 gas turbine*

The inlet of the calculation domain coincides with the turbine outlet of the engine and the outlet of the propelling nozzle is the outlet of the domain. Since the afterburner duct due to the two types of radial flame holders may be divided into six rotation periodic parts the calculation domain is a 60° sector of the actual afterburner duct. The domain contains two radial flame holders, flame holder ring, center cone and by pass air mixer.

The boundary conditions used for inlets and outlets of the calculation domain in the linear Euler solver are subsonic inlet and supersonic outlet respectively. According to Eriksson [8] well-posed boundary conditions for these types of boundaries is to for the subsonic inlet specify total pressure, total temperature and velocity direction at the boundary and for the supersonic outlet not specify anything.

An Euler grid created in P-CUBE was used in the linear Euler solver. The mean flow field that the equations governing the development of the perturbation field were linearized about was interpolated from a solution made earlier at VAC using the commercial CFD code FLUENT on an unstructured grid.

7.1 Mesh generation

A quite simplified geometry was created in GAMBIT a CAD and mesh generation tool that comes with the FLUENT solver. GAMBIT is mainly a tool for generation of unstructured grids and it was difficult to generate a structured grid of the domain. Since the linear Euler solver that was to be used in the eigenmodes extraction routine demands block-structured grids a tool better suited for generation of structured grids were tested. The created geometry was transferred to the mesh generation tool P-CUBE where a multi block structured grid of the calculation domain were created. The mesh generated is built up of 64 blocks and has a total of 131864 cells. The walls of the 60° sector is shown in figure 7. Figure 8 shows the center cone and flame holders after rotation a complete revolution.

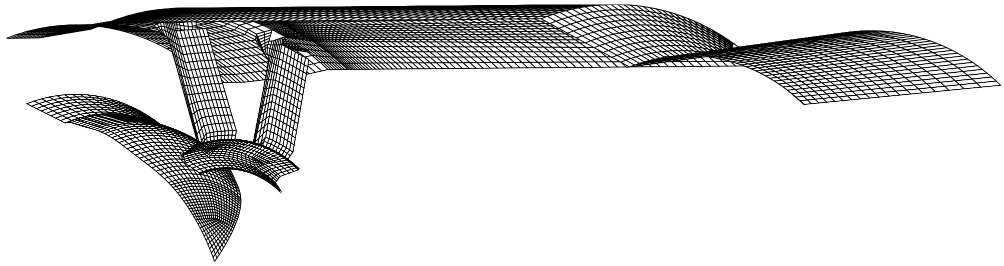

Figure 7 *Walls of the calculation domain.*

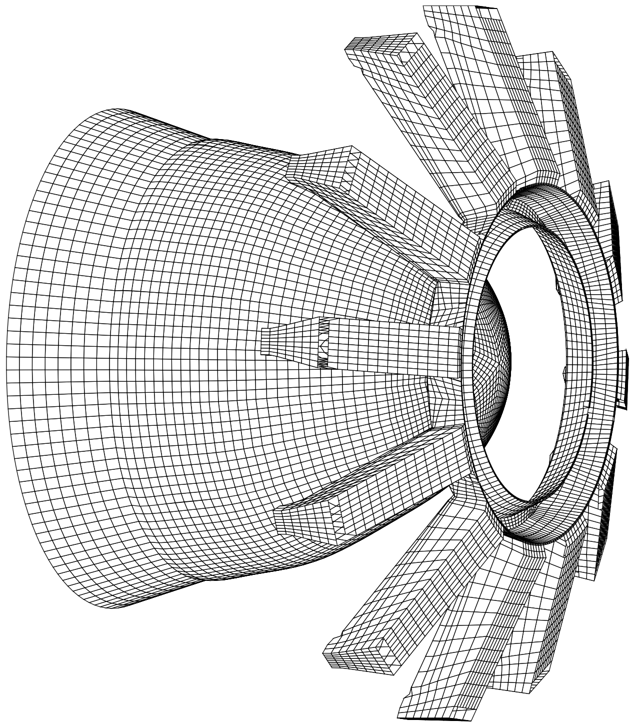

Figure 8 *Center cone and flame holders. The sector walls have been rotated to complete a whole revolution.*

The sector shape of the domain gives rise to singularity problems. To avoid these problems diamond shaped blocks are used in the center of the domain, see figure 9. The effect of using such blocks is that tangentially placed nodes are transformed to radial placed nodes on the opposite side of the block.

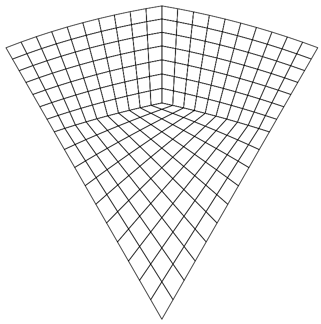

Figure 9 *Diamond shaped blocks are used to solve the singularity problem at the symmetry line of the domain.*

The same type of diamond shaped blocks is used beneath the radial flame holders to be able to place nodes on the rear side of them. The problem is that the number of nodes in the tangential direction in front of the flame holders must be the same above and below the flame holders. To be able to place nodes on the backside of the flame holders the number of nodes above them must be greater than the number of nodes below. By using diamond shaped blocks beneath the flame holders some of the tangential nodes are transformed to a radial position and thus it is possible to have more tangential nodes above the flame holder than below which solves the problem, se figure 10. The diamond shaped blocks gives rise to some cells with high skewness. High skewness is of course not recommended but the skewed cells might not have as great importance when using the mesh in a linear Euler solver as it should have had if it were to be used for calculation of a flow field with Navier-Stokes solver. In this case it is of greater importance to be able to create a mesh not too complex and with as few cells as possible than to create a mesh with high smoothness due to the fact that the eigenmode analysis is quite CPU time demanding.

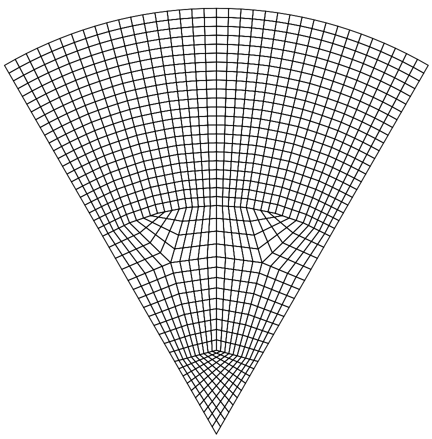

Figure 10 *Diamond shaped blocks are used to be able to place nodes on the rear side of the flame holder.*

7.2 Interpolation

The mean flow field that the equations governing the development of the perturbation field is to be linearized about were interpolated from an earlier calculation made at VAC with FLUENT using corresponding geometry and an unstructured mesh far more detailed then the structured mesh created in this case. The interpolation of properties from the unstructured mesh to the structured mesh used by the linear Euler code were, for each cell center in the structured mesh, performed in two steps. The first step was to find the four nodes in the unstructured mesh that were closest to the cell center in the structured mesh which values should be interpolated to. The second step was to perform the interpolation from the four nodes to the cell center in the structured mesh. To enhance the search process the calculation domain was broke down into a number of cubes. The search for nodes to be used in the interpolation was now limited to the cube in which the current cell center was located and the nearest surrounding cubes.

A coordinate system, (ξ,η,ζ), was created with the vectors $\overline{P_1P_2}$, $\overline{P_1P_3}$, $\overline{P_1P_4}$ as base vectors where P_1, P_2, P_3 and P_4 are the four nearest nodes in the unstructured mesh, see figure 11.

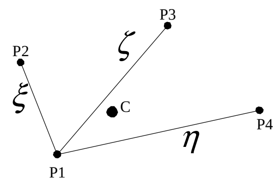

Figure 11 *The cell center C in the structured mesh and the nodes P_1-P_4 from the unstructured mesh.*

The mapping from the (ξ,η,ζ)-system to the (x,y,z)-system is described by the following expressions:

$$\begin{cases} x = (1-\xi-\eta-\zeta)\cdot x_1 + \xi\cdot x_2 + \eta\cdot x_3 + \zeta\cdot x_4 \\ y = (1-\xi-\eta-\zeta)\cdot y_1 + \xi\cdot y_2 + \eta\cdot y_3 + \zeta\cdot y_4 \\ z = (1-\xi-\eta-\zeta)\cdot z_1 + \xi\cdot z_2 + \eta\cdot z_3 + \zeta\cdot z_4 \end{cases} \tag{9.1}$$

Or in matrix form

$$\begin{bmatrix} (x-x_1) \\ (y-y_1) \\ (z-z_1) \end{bmatrix} = \begin{bmatrix} (x_2-x_1) & (x_3-x_1) & (x_4-x_1) \\ (y_2-y_1) & (y_3-y_1) & (y_4-y_1) \\ (z_2-z_1) & (z_3-z_1) & (z_4-z_1) \end{bmatrix} \begin{bmatrix} \xi \\ \eta \\ \zeta \end{bmatrix}, \mathbf{x} = \mathbf{Ab} \tag{9.2}$$

If det**A** $\neq 0$ the nodes from the unstructured mesh, P_1 to P_4, gives rise to a tetrahedron in (ξ,η,ζ)-space, see figure 12.

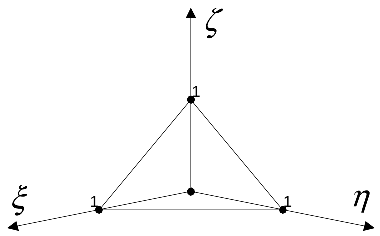

Figure 12 *The four nodes from the unstructured mesh gives rice to a tetrahedron shaped area in* (ξ,η,ζ) *-space.*

The coordinates for the cell centers in the (ξ,η,ζ)-system are determined with Cramers rule. That is $\mathbf{b}_j = \det\mathbf{A}_j / \det\mathbf{A}$ where j denotes that the j^{th} column in $\mathbf{A}$ has been replaced with $\mathbf{x}$. Interpolation is performed if the following criteria are fulfilled:

$$\begin{cases} \det A \neq 0 \\ \xi \geq -\varepsilon \\ \eta \geq -\varepsilon \\ \zeta \geq -\varepsilon \\ (\xi+\eta+\zeta) \leq (1+\varepsilon) \end{cases} \quad \text{, Where } \varepsilon = 0.2 - 0.3. \tag{9.3}$$

That is if the nodes from the unstructured mesh describe a tetrahedron in (ξ,η,ζ)-space and if the cell center, which values should be interpolated to, is situated within that same tetrahedron with some tolerance ε. Otherwise the cell center in the structured mesh get the same values of the properties as the nearest node in the unstructured mesh, i.e. interpolation of order zero is applied.

7.3 Inputs for linear Euler and Arnoldi

The largest time step that were found to be stable when running the linear Euler solver with the interpolated flow field as mean flow field was 0.5 μs which is a very small time step compared earlier two dimensional calculations made at VAC. To be able to compare the results from the calculations made in this thesis with the ones made earlier the total time step each time using the linear Euler solver in the Arnoldi routine were to be the same. Therefore the numbers of iterations made with the linear Euler solver for each vector created in the Krylov-Hessenberg sequence were set to 3000, i.e. a total time step of 1.5 ms. The start vector used in the Krylov-Hessenberg sequence was obtained by running the linear Euler solver 4000 iterations with a initial perturbation in ρu. The eigenvalues were found to be quite converged with a Krylov subspace containing 80 vectors. This should be compared with the total number of degrees of freedom of the system 1186776.

7.4 Results

The eigenmodes corresponding to interesting frequencies were picked out. To verify the estimated frequencies of the eigenmodes the linear Euler solver were started with eigenmodes as initial perturbation fields. After every iteration the pressure perturbations in one point of the calculation domain were saved. After a number of iterations corresponding to one full period or as for the lowest frequencies a quarter of one period a pressure-time diagram were set up.

Generally speaking all of the eigenmodes extracted were of growing character and most of them were growing with a quite high amplification. This is not the result expected. The two-dimensional calculations made earlier have given weakly damped or weakly amplified eigenmodes as result. Though the amplification was not to well agreeing with the amplification in the two-dimensional case the frequencies are almost the same.

Some of the eigenmodes with high amplification were real modes and they looked as if they were a result of the boundary conditions used. The boundary conditions were changed to a set of safer boundary conditions that are founded on zero-order extrapolation of the properties at the boundary. The change of boundary conditions gave eigenmodes with almost as high amplification as those extracted before.

The eigenmodes with frequencies most similar to those extracted in two-dimensional calculations are presented in table 2. It should be noted that all the five eigenmodes in table 2 are extremely amplified. Some of the eigenmodes extracted in two-dimensional eigenvalue analysis are represented in table 3.

Frequency [Hz]	Amplification per period
101.92	6.8E10
103.43	5.8E10
164.72	347.3385
390.42	21.0241
1028.44	5.5077

Table 2 *Frequencies and damping of eigenmodes estimated with the interpolated flow field.*

Frequency [Hz]	Amplification per period
110.2	0.177
198	0.594
277	0.824
379	1.037
467	0.864
552	0.823
788	0.894

Table 3 *Frequencies and damping of eigenmodes estimated in two-dimensional calculations made at VAC.*

Figure 13-17 shows the pressure perturbation fields corresponding to the eigenmodes in table 2. The pressure perturbation fields may be represented by pressure contour plots in an axial plane of the afterburner duct. The real part and imaginary part of each eigenmode are depicted in the figures. The imaginary part of an eigenmode represents the real part after one fourth of a whole period.

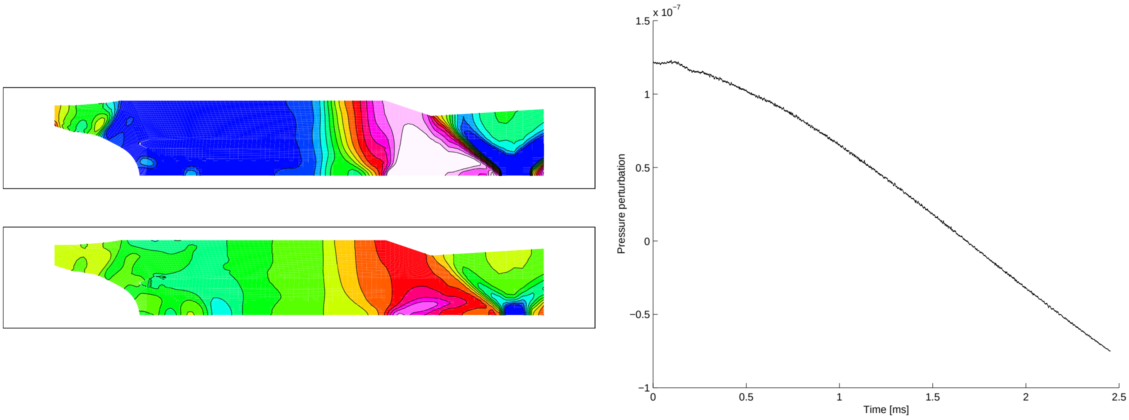

Figure 13 *Eigenmode with the frequency 101.92 Hz. The upper left picture shows the real part of the pressuremode and the lower left picture shows the imaginary part. The picture to the right shows the frequency validation plot, i.e. the pressure development in time.*

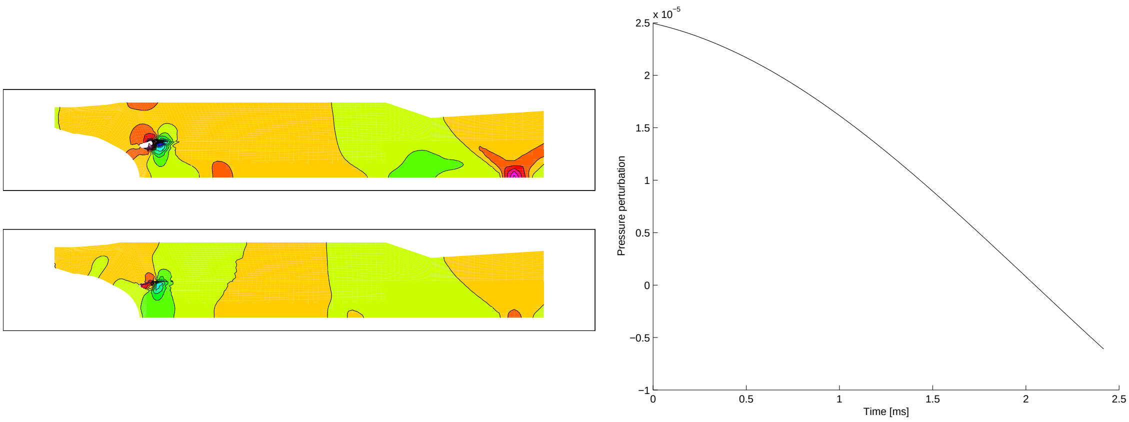

Figure 14 *Eigenmode with the frequency 103.43 Hz. The upper left picture shows the real part of the pressuremode and the lower left picture shows the imaginary part. The picture to the right shows the frequency validation plot, i.e. the pressure development in time.*

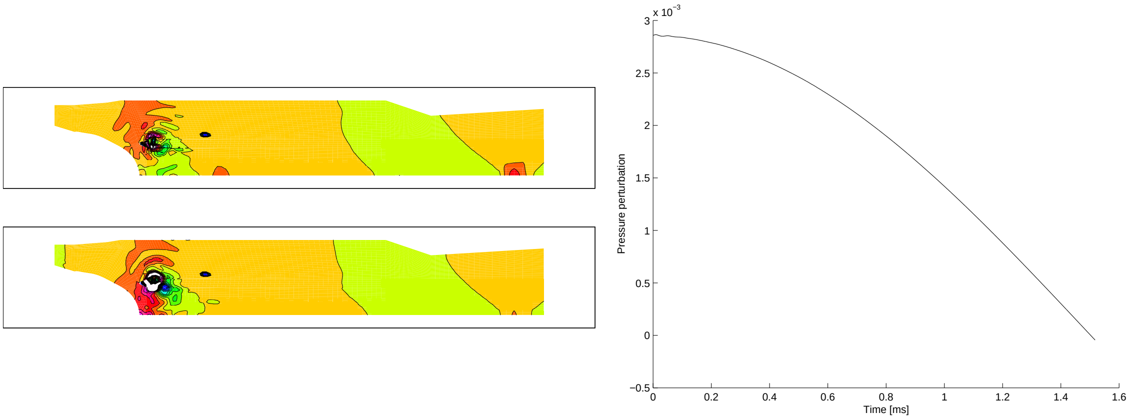

Figure 15 *Eigenmode with the frequency 164.72 Hz. The upper left picture shows the real part of the pressuremode and the lower left picture shows the imaginary part. The picture to the right shows the frequency validation plot, i.e. the pressure development in time.*

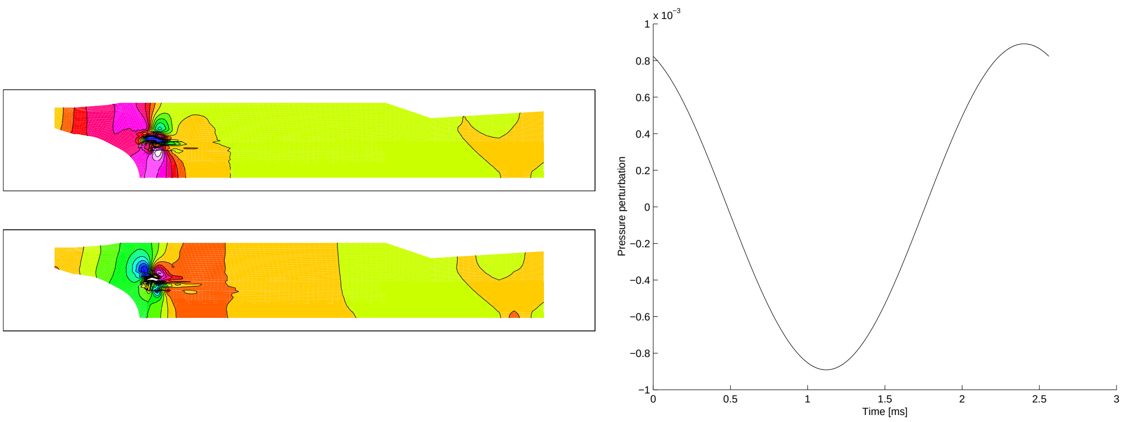

Figure 16 *Eigenmode with the frequency 390.42 Hz. The upper left picture shows the real part of the pressuremode and the lower left picture shows the imaginary part. The picture to the right shows the frequency validation plot, i.e. the pressure development in time.*

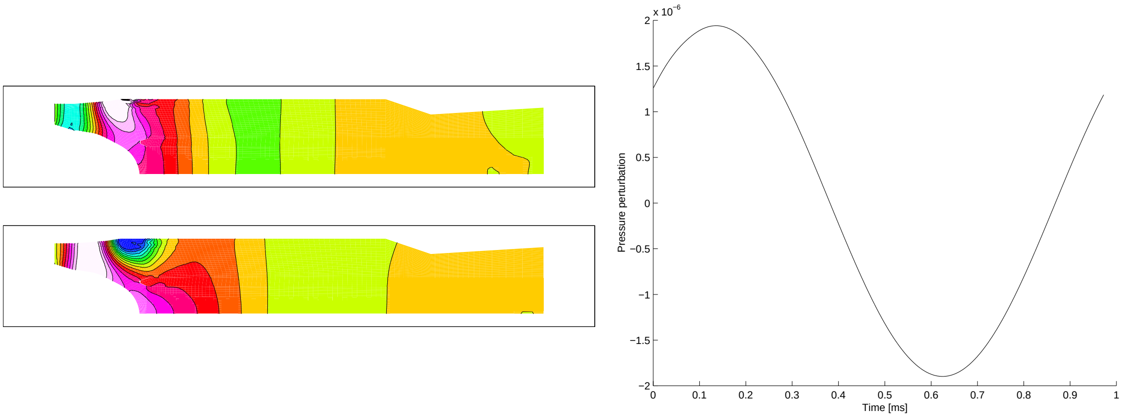

Figure 17 *Eigenmode with the frequency 1028.44 Hz. The upper left picture shows the real part of the pressuremode and the lower left picture shows the imaginary part. The picture to the right shows the frequency validation plot, i.e. the pressure development in time.*

7.5 Afterburner with stagnated fluid

To investigate if the non-physical eigenmodes were a result of numerical difficulties the eigenmode extracting routine was applied on the same calculation domain but with a stagnated mean flow field. It were found that the linear Euler solver were stable for a time step 5 times the time step used for the interpolated flow field. The total time step was kept constant which means that the number of iteration could be reduced with a factor 5. In this case no combustion takes place in the afterburner duct and the only fluid concerned is air. The total number of degrees of freedom decreases to 791184. In this case 90 vectors were obtained in the Krylov-Hessenberg sequence.

The eigenmodes extracted in this case were all damped. This indicates that the compatibility between the linear Euler solver and the mean flow field used in the linearization is quite important for the result.

The 90 extracted eigenmodes is well represented by the four eigenmodes in table 4.

Frequency [Hz]	Amplification per period
150.29	0.8690
230.05	0.9129
370.17	0.9409
926.85	0.9624

Table 4 *Frequencies and damping of eigenmodes in the estimated with the stagnated flow field.*

Figure 18-20 shows the pressure fields corresponding to the four eigenmodes. The three first eigenmodes are low frequency axially distributed modes and may be represented by contour plots in axial planes of the afterburner duct. The eigenmode in figure 20 is a high frequency mode with radial distribution. The plots of this eigenmode are therefore completed with contour plots in a radial plane. For all eigenmodes the imaginary part is almost zero. This indicates that the modes represent standing waves in the afterburner duct.

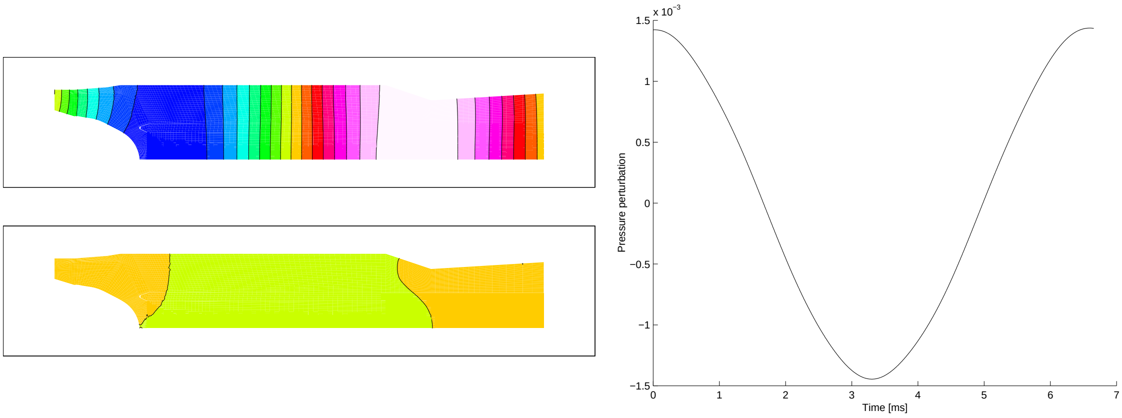

Figure 18 *Eigenmode with the frequency 150.29 Hz. The upper left picture shows the real part of the pressuremode and the lower left picture shows the imaginary part. The picture to the right shows the frequency validation plot, i.e. the pressure development in time.*

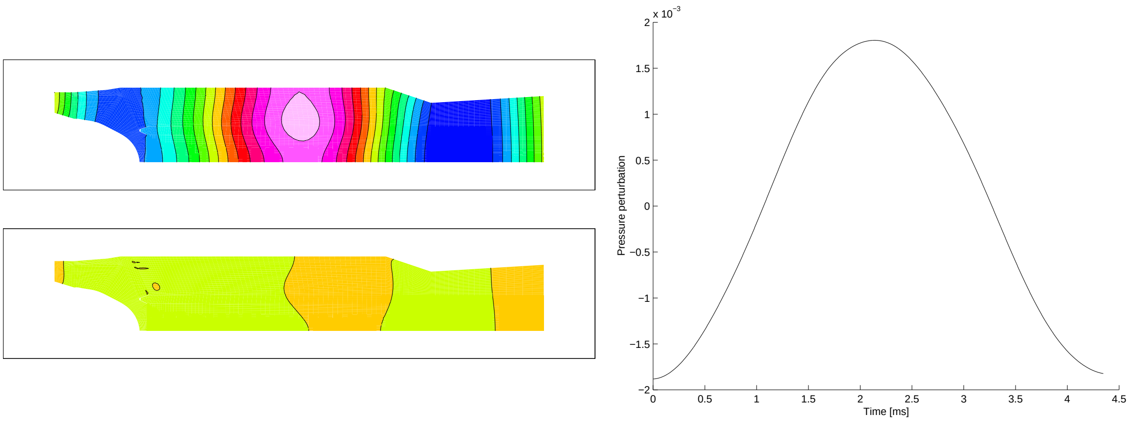

Figure 19 *Eigenmode with the frequency 230.05 Hz. The upper left picture shows the real part of the pressuremode and the lower left picture shows the imaginary part. The picture to the right shows the frequency validation plot, i.e. the pressure development in time.*

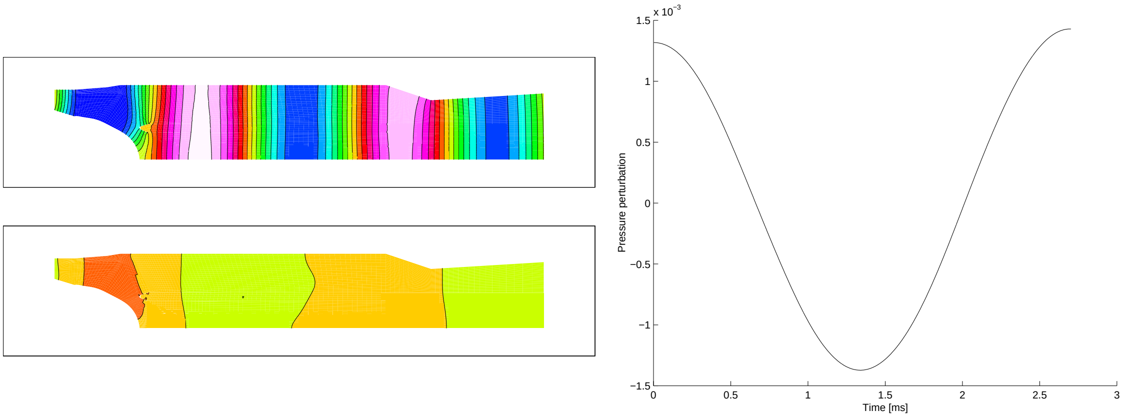

Figure 20 *Eigenmode with the frequency 370.17 Hz. The upper left picture shows the real part of the pressuremode and the lower left picture shows the imaginary part. The picture to the right shows the frequency validation plot, i.e. the pressure development in time.*

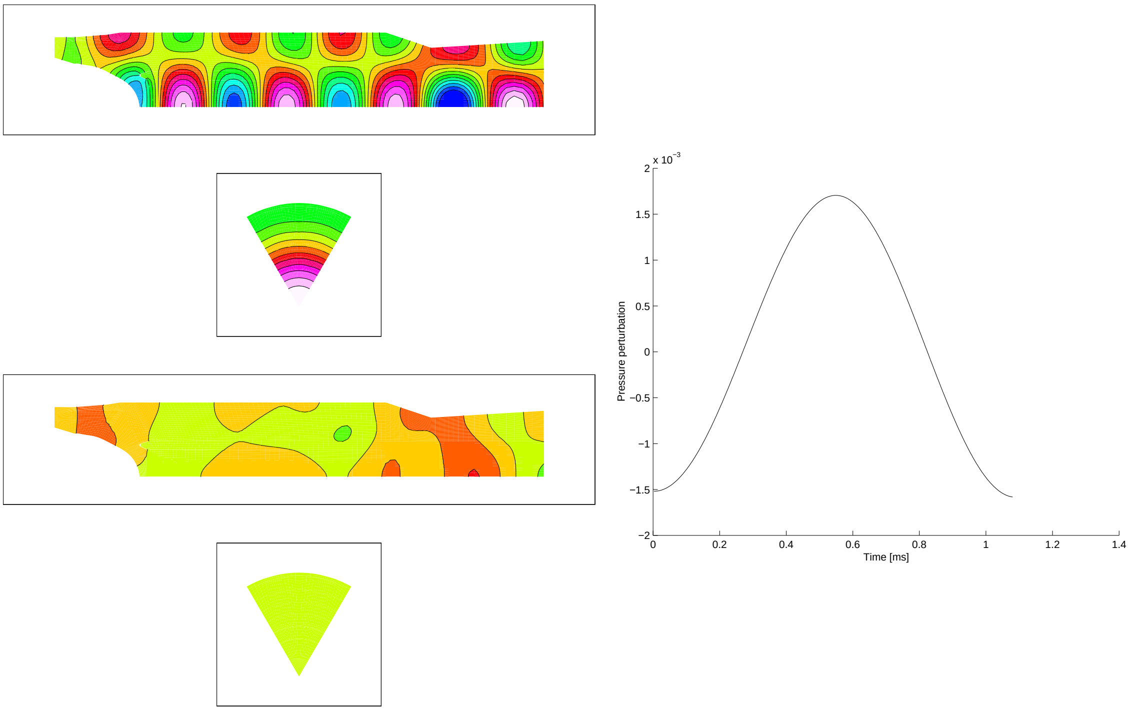

Figure 21 *Eigenmode with the frequency 926.85 Hz. The two upper left pictures show the real part of the pressuremode and the two lower left pictures show the imaginary part. The picture to the right shows the frequency validation plot, i.e. the pressure development in time.*

7.6 Stability analysis

In the eigenmode analysis the effects of variation in heat release has been ignored. This means that a phenomenon that may lead to augmentation of the modes, which may cause natural oscillations, has been left out of the analysis. The analysis above therefore has to be completed with an investigation of such behaviors. For the low frequency rumble modes Rayleigh's criteria may be used. The criteria say that if the pressure variations are in phase with the variations of heat release positive feedback will occur in the system, Eriksson [9]. Reverse phase of the variations results in negative feedback of the system. The variations in heat release only occur in flame regions of the afterburner duct i.e. the area where most of the reactions take place. The rate of reaction of the mean flow field is a god indication of such chemical activity. That is the variations of heat release may be expressed as the variations in equivalence ratio multiplied with the rate of reaction in the mean flow field, Eriksson [9]. In the FLUENT solver, which has been used to obtain the mean flow field, the eddy dissipation Magnussen and Hjertager model for rate of reaction was adopted, [12]. The rate of reaction is given by the smaller, i.e. the limiting value, of the expressions below:

$$R_{i',k} = \upsilon'_{i',k} M_{i'} A\rho \frac{\varepsilon}{k} \frac{m_R}{\upsilon'_{R,k} M_R} \tag{9.1}$$

$$R_{i',k} = \upsilon'_{i',k} M_{i'} AB\rho \frac{\varepsilon}{k} \frac{\sum_P m_P}{\sum_{j'}^{N} \upsilon''_{j',k} M_{j'}} \tag{9.2}$$

where

N is equal to the number of species.
$\upsilon'_{i',k}$ represents the stoichiometric coefficient for reactant *i'* in reaction *k*.
$\upsilon''_{i',k}$ represents the stoichiometric coefficient for product *i'* in reaction *k*.
m_P represents the mass fraction of any product species, *P*.
m_R represents the mass fraction of a particular reactant, *R*.
R is the reactant species giving the smallest value of $R_{i',k}$.
A is an empirical constant equal to 4.0
B is an empirical constant equal to 0.5

The stochiometric reaction of interest is fuel completely combusted with oxygen as oxidizer and carbon dioxide and water as the only products.

$$C_n H_m + \left(n + \frac{m}{4}\right) O_2 \rightarrow nCO_2 + \frac{m}{2} H_2O \tag{9.3}$$

The subscripts *n* and *m* defines the fuel used. In the case of the RM12 afterburner *n=12* and *m=23* which gives

$$C_{12}H_{23} + 17{,}5\,O_2 \quad \rightarrow \quad 12\,CO_2 + 11{,}5\,H_2O \tag{9.4}$$

A correlation between the pressure perturbation field and the heat release perturbation field may be expressed as:

$$c = \frac{P' \bullet R_{i',k}\Phi'}{\left\| P' \right\| \left\| R_{i',k}\Phi' \right\|} \tag{9.4}$$

Where c is the phase angle between the pressure fluctuations and the fluctuations in heat Release. In (9.4) the numerator is defined by

$$P' \bullet R_{i',k}\Phi' = \int_{\Omega} P' R_{i',k}\Phi' \, dV \tag{9.5}$$

And the denominator by

$$\left\| P' \right\| = \sqrt{P' \bullet P'} \;\; ; \;\; \left\| R_{i',k}\Phi' \right\| = R_{i',k}\sqrt{\Phi' \bullet \Phi'} \tag{9.6}$$

In (9.4) – (9.6) *P'* denotes pressure fluctuations and *Φ'* denotes fluctuations in equivalence ratio.

This stability analysis applied on the eigenmodes obtained using the interpolated flow field gives the result tabulated in table 5. Since the eigenmodes are not physically correct these results are not valid for the actual afterburner.

Frequency [Hz]	c, phase angle
101.92	-1.87964E-02
103.43	6.12658E-02
164.72	-0.2827
390.42	1.05099E-02
1028.44	1.41553E-04

Table 5 *Phase angle between pressure and heat release perturbations.*

8 Computing time and data storage requirements

The calculations in the eigenmode extraction routine were done with an Arnoldi embedded linear Euler solver for single processor and were performed on a Hewlett Packard J2240 236 MHz workstation.

With the interpolated flow field as mean flow field the CPU-time for each iteration with the linear Euler solver was 7 seconds. In this case each vector created in the Arnoldi routine means 3000 iterations with the linear Euler solver. Thus the total CPU-time per vector in the Krylov subspace equals 21000 seconds calculation time. The Arnoldi routine was found to generate quite converged eigenvalues for a Krylov sub space containing 80 vectors. The total CPU-time required to obtain this sub space is 470 hours or roughly 20 days. The memory usage for each vector is 4.6 MB and thus the total memory usage for the entire Krylov sub space is 368 MB.

When the mean flow field was replaced by stagnated fluid the solver was found to be stable for a time step five times the time step used with the interpolated flow field. Thus the number of iterations were decreased with a factor five. Since this flow field does not involve any combustion and not as many species both the memory usage and the CPU-time is somewhat smaller. The CPU-time for each iteration with the linear Euler solver was 5 seconds and the total time for every vector 3000 seconds. 90 vectors were generated and thus the total CPU-time for the Arnoldi process in this case was 75 hours. The memory usage for each vector is 3 MB and for the entire sub space 270 MB.

If the eigenmode extraction routine were applied on a mean flow field compatible with the solver used the calculation time would most probably be somewhere in between the time for the interpolated flow field and the time for the stagnated flow field.

9 Conclusions

The interpolated mean flow field constitutes a not too well converged solution for the mesh and solver used in the eigenmode extraction routine. The governing equations has therefore been linearized about a non-convergent solution and the eigenmodes extracted corresponds to the course of events taking place soon after the starting of the solver with the mean flow field as start solution, i.e. large fluctuations in residuals and excitation of numerical eigenmodes. Looking on the extracted eigenmodes one might see that certain areas seems to be farther from convergence than other. Much of the activity in the eigenmodes is focused in the areas around the flame holders.

Though the eigenmodes do not seem to be physical the frequencies are in the same regions as those obtained in two-dimensional calculations made at VAC. This might indicate that the acoustic behavior of the geometry used is well predicted even though the eigenmodes are not.

The case with stagnated reference flow shows that the method gains physically correct eigenmodes and that the above described problems are not due to any errors in the linear Euler solver or the Arnoldi algorithm.

It seems like it is important to have a good compatibility between grid, solver and mean flow field to be able to perform a successful eigenmode extraction. Thus one would need to obtain a well-converged mean flow field using a viscous solver that is compatible with the linear Euler solver used in the eigenmode extraction routine. One way of doing this is to perform all calculations with the same grid. The problem with this is that one has to run the linear Euler solver on a Navier-Stokes grid, i.e. a grid with finer mesh in the boundary layers to be able to resolve viscous effects. This means that the linear Euler solver has to be used together with a mesh unnecessarily detailed which is not desirable due to long calculation times. This also means that some work has to be done developing a grid to grid interpolating routine that ensures that the interpolated flow field is compatible with the destination solver and grid and that it constitutes a converged solution.

10 Future work

The results off this work shows that if the method is going to be used for eigenmode extraction the interpolation routine has to be improved with some kind of technique that makes the interpolated flow field compatible with the destination grid and solver. The flow field has to be a converged solution in the linear solver to be used.

Care should be taken to impose physically correct boundary conditions so as not to corrupt the eigenvalues and eigenmodes.

The Euler grid created in this work might need some refinement and smoothening to make some cells less skewed.

The eigenmode extraction process is quite CPU demanding and therefore it would be a good idea to modify the codes and thereby make it possible to perform parallel computing.

To enhance the eigenmode extraction routine it would be preferable to have a good method of finding with which frequency a certain mode oscillates.

Bibliography

[1]. Banhawy, Y. El, Melling, A. and Whitelaw, J. H.: *Combustion Driven Oscillations in a Small Tube*. Combustion and Flame **33**, 281-290 (1978).

[2]. Bloxidge, G. J., Dowling, A. P., Hooper, N. and Langhorne, P. J.: *Active Control of Reheat Buzz*. AIAA Journal, Vol. **26**, No. 7, July 1988.

[3]. Bloxidge, G. J., Dowling, A. P., Hooper, N. and Langhorne, P. J.: *Reheat Buzz: an Acoustically Coupled Combustion Instability. Part 2*. Theory. J. Fluid Mech. (1988), Vol. **193**, pp. 445-473, G. B.

[4]. Campbell, I. G. and Moss, J. B.: *Combustion Oscillations in a Ducted Premixed Flame*. The University of Southhampton, Hampshire, 1983.

[5]. Darking, D. D., Radhakrishnan, K., Oyediran, A. and Cowan, E.: *Combustion-Acoustic Stability Analysis for Premixed Gas Turbine Combustors*. 1995. AIAA 95-2470.

[6]. Darling, D. D., Radhakrishnan, K. and Oyediran, A.: *Sensitivity of Combustion-Acoustic Instabilities to Boundary Conditions for Premixed Gas Turbine Combustors*. NASA Technical Memorandum 106890.

[7]. Eriksson, L. E.: *Development and validation of highly modular flow solvers in G2DFLOW and G3DFLOW series for compressible viscous reacting flow*. Technical Report 9970-1162, Volvo Aero Corporation, 1995.

[8]. Eriksson, L. E.: *Lecture Notes: Numerical Simulations of Compressible Flows*. 1999.

[9]. Eriksson, L. E.: *TMT/Brum och skrik*. Volvo Aero Corporation, 1999

[10]. Eriksson, L. E.: *Transfinite Mesh Generation and Computer-Aided Analysis of Mesh Effects*. Thesis for the degree of doctor of philosofy, Uppsala University, Department of Computer Science, 1984.

[11]. Fazal, B. K.: *An Overview of Gas Turbine Propulsion Technology*. California State Polytechnic University. 1994. AIAA 94-2828.

[12]. Fluent Inc.: Chemical Species Transport and Reacting Flow. User's Guide Volume 2, Fluent Incorporated, 1998.

[13]. Hendersson, B. E. and Lewis, J. S.: *Characteristics of Combustion Driven Pressure Oscillations in Advanced Turbo-Fan Engines with Afterburner*. NASA Technical Reports, 90N10194.

[14]. Hoffman, K. A. and Chiang, S. T.: Computational Fluid Dynamics for Engineers, Vol 2. ISBN:

[15]. Keller, J. J.: *Thermoacoustic Oscillations in Combustion Chambers of Gas Turbines*. AIAA Journal Vol. **33**, No. 12, December 1995.

[16]. Kuhn, T. E., Mongia, H. C. and Bruce, T. W.: *Small Turbine Engine Augmentor Design Methology*. 1982. AIAA 82-1179.

[17]. Macquisten, M. A. and Dowling, A. P.: *Combustion Oscillations in a Twin-Stream Afterburner*. 1993. AIAA 93-4392.

[18]. Macquisten, M. A. and Dowling, A. P.: *Low-Frequency Combustion Oscillations in a Model Afterburner*. Combustion and Flame **94**, 253-264 (1993).
[19]. Margolis, S. B.: *Nonlinear Stability of Combustion-Driven Acoustic Oscillations in Resonance Tubes*. Combustion Research Facility, Sandia National Laboratories, Livermore, California 94551 USA. 1992.
[20]. Oyediran, A., Darling, D. D. and Radhakrishnan, K.: *Review of Combustion-Acoustics Instabilities*. 1995. AIAA 95-2469
[21]. Panton, R. L.: *Incompressible Flow*. Wiley Interscience, 1996. ISBN: 0-471-59358-3.
[22]. Poinsot, T. J., Trouve, A. C., Veynante, D. P., Candel, S. M. and Esposito, E. J.: *Vortex-Driven Acoustically Coupled Combustion Instabilities*. J. Fluid Mech. (1987), Vol. **177**, pp. 265-292, G. B.
[23]. Richards, G. A. and Yip, J. M.: *Oscillating Combustion from a Premixed Fuel Nozzle*. U. S. Department of Energy, Morgantown Energy Technology Center, Morgantown, WV 26505. DOE/METC/C-95/7189.
[24]. Russel, P. L., Brant, G. and Ernst, R.: *Low-Frequency Augmentor Instabillity Study*. 1978. AIAA 78-996
[25]. Smith, D. A. and Zukoski, E. E.: *Combustion Instability Sustained by Unsteady Vortex Combustion*. 1985. AIAA 85-1248.
[26]. Versteeg, H. K. and Malalasekera, W.: *An Introduction to Computational Fluid Dynamics*. Longman Higher Education Division, 1994. ISBN: 0-582-21884-5.
[27]. Wilcox, D. C.: *Turbulence Modeling for CFD*. DCW Industries, 1998. ISBN: 0963605151
[28]. Yang, V. and Culick, F. E. C.: *Nonlinear Analysis of Pressure Oscillations in Ramjet Engines*. 1986. AIAA 86-0001.

Appendix (Flow properties)

Figure 22-31 below shows properties of the interpolated flow field used in Arnoldi's method. The plots are contour plots in an axial plane of the afterburner duct.

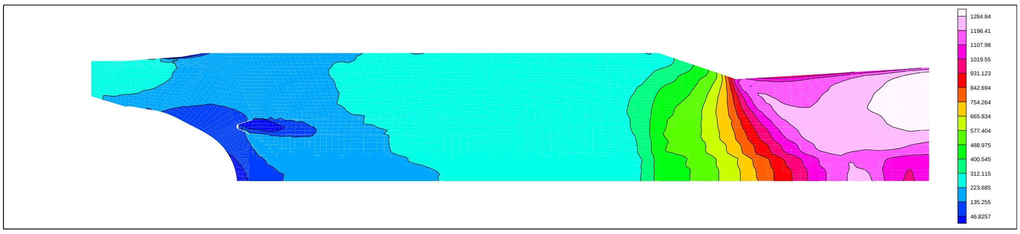

Figure 22 *Axial velocity, u.*

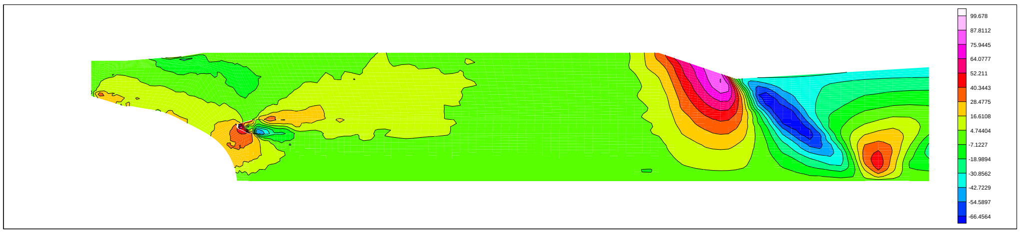

Figure 23 *Radial velocity, v.*

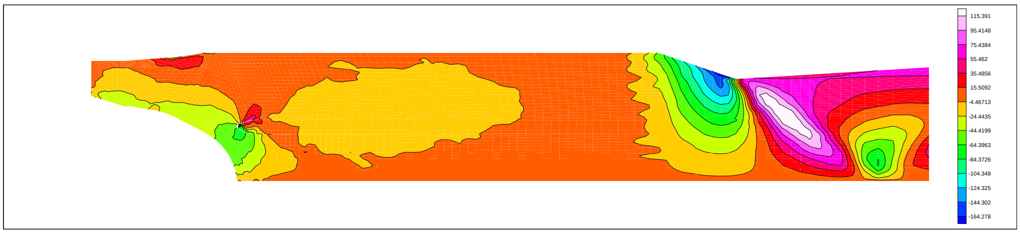

Figure 24 *Tangential velocity, w.*

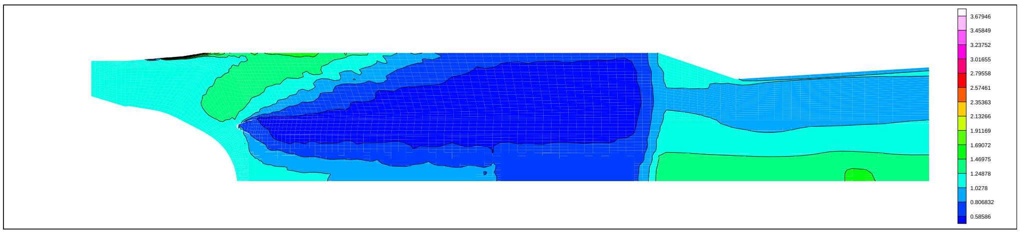

Figure 25 *Density.*

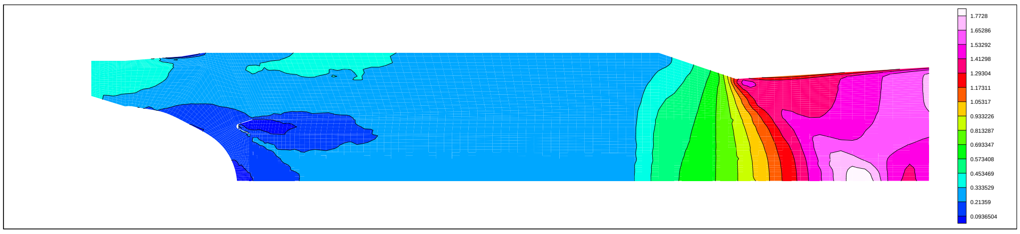

Figure 26 *Mach number*.

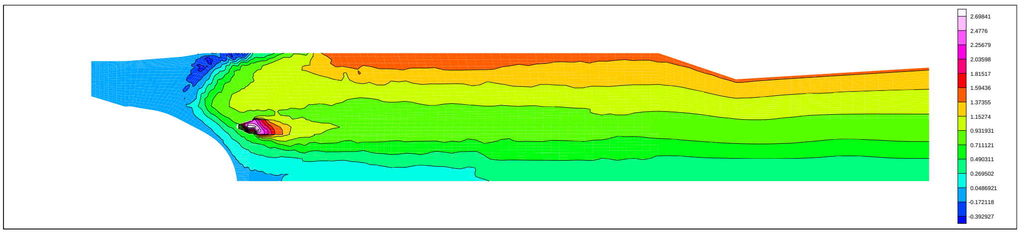

Figure 27 *Equivalence ratio.*

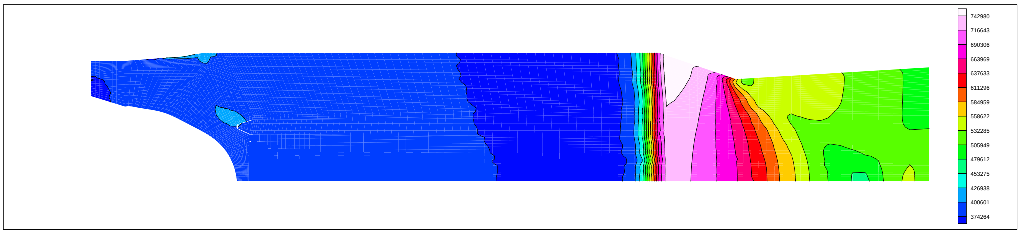

Figure 28 *Static pressure.*

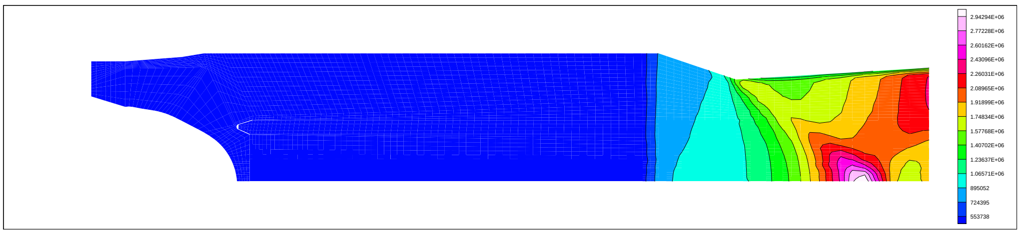

Figure 29 *Dynamic pressure.*

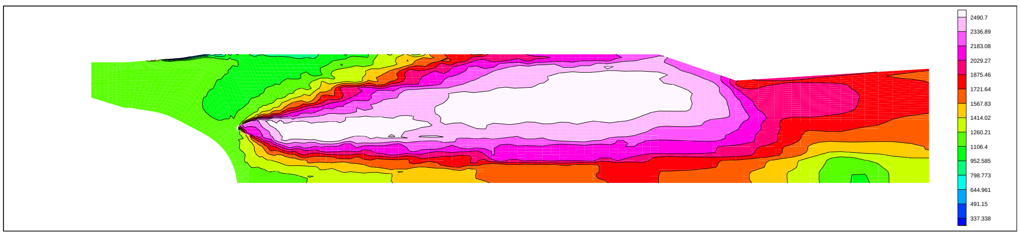

Figure 30 *Static temperature.*

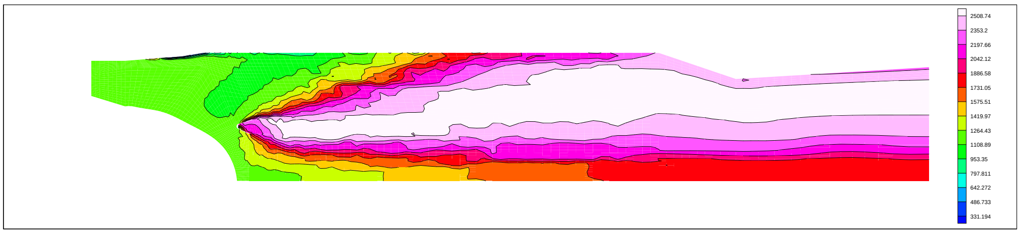

Figure 31 *Dynamic temperature.*